Correlation of 2GCHAS Analysis with Experimental Data

Joon W. Lim

Sterling Software
Moffett Field, California

Tassos Anastassiades

Advanced Rotorcraft Technology, Inc,
Mountain View, California

Abstract

A broad engineering validation study of the structural and aerodynamic capabilities of the Second Generation Comprehensive Helicopter Analysis System (2GCHAS) has been conducted. 2GCHAS predictions for structural deflections, aeroelastic stability, rotor performance, and blade airloads were compared with experimental data ranging from small-scale model data to full-scale wind tunnel and flight test data. Correlation with Princeton beam test data confirms that 2GCHAS gives satisfactory results for moderate deformations of nonlinear structures. A small-scale torsionally soft hingeless rotor blade test model was correlated with 2GCHAS aeroelastic stability results and confirmed 2GCHAS' capability to predict aeromechanical stability of a hingeless rotor system. For unsteady aerodynamics, 3-D wing dynamic stall wind tunnel data for an oscillating wing confirmed 2GCHAS dynamic stall and unsteady wake modeling capability. Rotor performance predictions were correlated with full-scale wind tunnel data for the S-76 rotor. Rotor blade loads and airloads predictions were evaluated using CH-47C model rotor blade data and UH-60 full-scale flight test data. Overall, the results indicate generally satisfactory prediction capabilities for a wide range of rotorcraft problems using 2GCHAS.

Presented at the American Helicopter Society Aeromechanics Specialists Conference, San Francisco, California, January 19-21, 1994.

Introduction

The Second Generation Comprehensive Helicopter Analysis System (2GCHAS) is a multi-disciplinary, user-friendly comprehensive rotorcraft analysis code. Its structural analysis capability is finite element based and the element library includes nonlinear beam, linear beam, and rigid body mass elements. The 2GCHAS user can build a complete structural model by selecting various finite elements from the element library. Numerous aerodynamic options are available such as linear, nonlinear (table look-up) and unsteady aerodynamics, prescribed and free wakes, a generalized dynamic wake, and various aerodynamic interference options. The interface between structural and aerodynamic models is a user input option. This feature allows the user to easily access various functionalities. In addition to the user-friendly 2GCHAS environment, this correlation study will confirm the promising capability of 2GCHAS comprehensive analysis as well as enhance understanding of the physics of the experimental data.

A 2GCHAS comprehensive rotorcraft analysis involves nonlinear structural and aerodynamic analyses coupled with unsteady airloads and wake effects. The rotating blade makes the rotorcraft analysis inherently more complicated and also significantly increases the size of the system, so that the analyst requires numerically efficient algorithms. The situation becomes more difficult for correlation analyses since many newly designed rotor blades experience moderate or large structural deformation in addition to complex 3-D dynamic stall phenomena. The objective of the 2GCHAS software development has addressed these issues and

correlation with experimental data is necessary to insure the success of its integrated functionality.

A full description of 2GCHAS is given in the System documentation, Ref. 1--3. Other publications dealing with the development and evolution of 2GCHAS include Refs. 4--12. A companion paper, Ref. 13, gives an overview of the current version of 2GCHAS and the latest results from applying the analysis to complex rotorcraft configurations.

Engineering Validation

The Second Generation Comprehensive Helicopter Analysis System (2GCHAS) is an interdisciplinary software system that has been developed to integrate the major rotorcraft analysis capabilities to provide analytical capabilities for researchers, designers, and evaluators across a spectrum of major rotorcraft technical disciplines. The 2GCHAS development has included extensive system testing and has been released to the user community, however only limited engineering validation has been conducted to date.

Engineering validation is a key part of the 2GCHAS development process and is essential to the successful utilization of 2GCHAS. The usefulness and success of any rotorcraft analysis depends on its capabilities and accuracy; user confidence in these attributes can only be established when sufficient demonstrations of the validity of the analysis results are achieved. The objectives of 2GCHAS engineering validation are to demonstrate the accuracy, validity, and capabilities of the system as well as identify voids in capability or deficiencies when they exist.

Engineering validation differs from the software testing carried out in the development process prior to release of the system. Software testing is primarily intended to eliminate software coding errors and insure that software units operate correctly together as a system so that the system produces numerical results that are consistent with the mathematical equations coded in the software. However, since the mathematical model is to some degree an approximation of the actual rotorcraft physical system and its fluid environment, 2GCHAS numerical results also need to be compared with experimental measurements of real-word vehicles to establish the degree of validity of assumptions and approximations contained in the math model. Only by comparison with actual test data is it be possible to assess the impact of these approximations on the overall accuracy of the results.

In principle, engineering validation is a straightforward procedure but it must be done with considerable care, otherwise the validation will lack authority and user confidence will suffer. Experimental data sets require special considerations in validation of comprehensive analyses. In addition to measured data, the physical properties of the vehicle must also be accurately known. Comparison data must be selected carefully from a wide variety of data set types. These may represent a complete rotorcraft or only a single component of the system. Full-scale flight test data affords the most realistic conditions to exercise the analysis. However, ensuring accuracy and validity of the data is not a trivial task, especially for flight test conditions.

The experimental data sets chosen for the correlations presented in this paper include nonlinear beam static structural response, hingeless rotor blade aeroelastic stability, coupled rotor body aeromechanical stability, dynamic stall aerodynamics, and full scale rotor performance and rotor loads. The experimental data used for correlations were chosen based on reliability and availability of the data. Some data were for the small scale model blades, and some were for the full scale rotor blades in the wind tunnel as well as free flight.

Static Deflection of a Nonlinear Beam

The 2GCHAS nonlinear beam finite element is based on the Hodges-Dowell theory, Ref. 14. The Princeton beam experiments of nonlinear beam structural response (Ref. 15) are commonly employed to validate nonlinear analyses for beams experiencing large deformations. The Princeton beam test model represents a simple cantilevered beam under a gravity load from a concentrated mass at the tip, undergoing large flap, lag and torsional deflections. The experimental beam model was a rectangular cross-section, uniform aluminum beam 20 in. long, 1/2 in wide, and 1/8 in. thick. Under the static gravity load, the initial pitch angle was varied so that the loading angle between the beam chord axis and the gravity load varied from 0 to 90 degrees. Since the beam was slender, it experienced

relatively large flap, lag, and torsional deformations due to the gravity tip loads.

2GCHAS Analysis

The beam was modeled in 2GCHAS using six nonlinear beam elements. Each element has fifteen degrees of freedom, with twelve degrees of freedom representing the translations and rotations at the end nodes, and the remaining three degrees of freedom representing axial and torsional deformations in the beam interior. A mechanical load element was used to represent the concentrated tip weight.

An important difference between the 2GCHAS nonlinear beam element and the Hodges-Dowell element, which had a significant impact on the element's development and the correlation results, should be noted: the Hodges-Dowell equations contained a special parameter for the pitch control input. In 2GCHAS, this input is treated as ordinary torsion degree of freedom, which is necessary when a control system is present and the input is a variable rather than a prescribed quantity. As a result, in the original element the pitch control angle was subject to the same ordering scheme restriction as the Hodges-Dowell elastic torsion angle and was too restrictive. To overcome this restriction, an upgraded element was developed in which the ordering scheme on the torsion degree of freedom, but not its spatial derivative, is relaxed entirely, although the Hodges-Dowell ordering scheme is retained for transverse bending rotations.

In the experiment, the angle between the load and chord varied from zero degrees to ninety degrees. In the analysis, two methods were used to vary the direction of the load relative to the beam chord. In the first method, the orientation of the undeformed model was kept fixed and the direction of the applied load was varied so that the angle between the chord and the load matched the experiment. In the second method, the orientation of the applied load was kept fixed, but the beam was rotated relative to the load by specifying the pitch control at the base of the beam.

Correlation Results

The results are shown for the three separate cases, in Fig. 1a-c. Results are included for two bending deflections and torsion and for three levels of applied loads. The first results, Fig. 1a, are for the case where the angle of the load with respect to the beam was varied so that the beam orientation remained constant. In the second case, the load angle is held constant, and the pitch angle of the beam was varied. Two sets of results here are given for both the original beam model, Fig. 1b, and the upgraded beam model, FIg. 1c. The good results for both elements when the load angle varies are to be expected because the magnitudes of all deflections fall within the Hodges-Dowell ordering scheme, which limits all deformations of the original element, but applies only to the translational deformations of the new element. The correlation between theory and experiment is different when the pitch angle varies, because the pitch control is applied to the torsional degree-of-freedom at the base of the beam. Consequently, the torsion degrees-of-freedom of the finite element model must absorb the rigid body pitch motion induced by the pitch control input as well any elastic torsional deformation relative to that motion. The Hodges-Dowell ordering scheme for the torsion angle is always violated when the control pitch exceeds about 8 degrees, and the consequences of this are apparent in the poor correlation of bending deformations with experiment for the original beam element. The upgraded element shows significantly improved correlation with experiment for large control pitch angles, which is to be expected because the restrictions on torsional rotations have been lifted. Paradoxically, the torsional motions predicted by the original element are slightly better than the predictions of the new element for intermediate control pitch inputs, although the new element correctly predicts that torsion must vanish when the control input is at 90 degrees.

Hingeless Rotor Blade Aeroelastic Stability

In Ref. 16, Sharpe presented extensive data for a small-scale torsionally soft hingeless rotor (TSR) model that provides an excellent fundamental test of the basic nonlinear structural dynamics and aeroelastic stability prediction capabilities of any rotorcraft prediction analysis, and particularly those based on finite element methods. The availability of data for variations of precone and droop for a blade having high torsional flexibility insures that the structural coupling characteristics that govern hingeless rotor aeroelastic stability will be fully exercised. This data was used to compare with results of eight different analysis codes from industry and government as a part of ITR

methodology assessment workshop, Ref. 17. For the cases without precone or droop, most of the analysis codes gave fair correlation of the lead-lag damping in the range of the low to medium collective pitch. However, the predictions deviated from the experimental data for large collective pitch angles. Recently, researchers (Ref. 18) have shown that more refined 3-D unsteady aerodynamic models could improve the lead-lag damping correlation at the higher blade pitch angles. The 2GCHAS results presented herein are limited to preliminary correlations with 2-D unsteady aerodynamics.

The torsionally soft rotor model (TSR) was specifically designed to provide aeroelastic data to validate hingeless rotor stability prediction codes. It is a simple stiff inplane hingeless rotor configuration with two torsionally soft blades and an optional root pitch flexure. It was designed to be as simple as possible to focus on the basic aeroelastic characteristics of interest and minimize experimental error or uncertainty regarding extraneous issues. Accordingly the blades were designed to be structurally simple, with uniform mass and stiffness properties, with coincident elastic, mass, and aerodynamic centroids. The model has two blades with a radius of 3.15 ft., a blade chord of 0.28 ft., and a symmetrical NACA 0012 airfoil. The model operates at a rotor speed of 1000 RPM with a tip speed of 330 ft/sec. The low Reynolds Number results in stall occurring at relatively low angles of attack but the data is reliable and repeatable at low thrust levels. The model was tested in the hover condition where lead lag excitations were induced and the resulting free oscillation transients were measured to determine the frequency and damping using the moving block technique.

2GCHAS Analysis

For the 2GCHAS analysis of this model, the cantilever blade was modeled with seven nonlinear beam elements clamped at the root. The torsion degree of freedom at the blade root is prescribed by the collective pitch control input. The blade pitch flexure was modeled by the spring element. The precone or droop was modeled by aligning the beam element nodes to correspond to the precone or droop angle. The aerodynamic model included seven aerosegments, and for the preliminary correlation given herein, linear unsteady aerodynamics coupled with uniform inflow was employed.

Correlation Results

Results are presented for the basic blade without precone or droop, and the frequency and damping of the lead lag bending degree of freedom are presented in Fig. 2. The correlation of the results is generally good except for the higher blade pitch angles where the effects of airfoil stall and 3-D unsteady aerodynamics become more important. The results for the cases with precone and droop are shown in Figs. 3 and 4, respectively. In each case, two plots are shown, one with the soft pitch flexure and the other with the stiff pitch flexure. The effect of the soft pitch flexure is to lower the torsion frequency of the blade and to increase the effective pitch-lag and pitch flap aeroelastic couplings arising from the nonlinear bending-torsion coupling characteristics of the cantilever rotor blade. Again the correlations are reasonably good and show the expected effects of the variations in the four different configurations. And again at the larger pitch angles, the results deviate from the experimental data due to aerodynamic effects not included in the analysis.

In order to focus more directly on the aeroelastic effects from nonlinear structural behavior without having to deal with the effects of nonlinear aerodynamics, the results are presented in Fig. 5 for the low collective pitch angle as an explicit function of the blade precone and droop angles. Here the effects of the structural characteristics on lead-lag damping are much more evident and the analysis is observed to behave in the appropriate manner.

The results of this correlation indicate that the basic aeroelastic effects of hingeless rotor blade structural dynamics represented by the finite element modeling capabilities of 2GCHAS are satisfactory. The effects of more advanced aerodynamic modeling included in the system will be addressed in more detailed correlations.

Coupled Rotor-Body Aeromechanical Stability

Aeromechanical stability of hingeless rotor helicopters involves dynamic coupling of fuselage with the rotor flap and lead-lag degrees of freedom together with significant aeroelastic coupling effects from blade structural properties and aerodynamics. A basic test of any aeroelastic analysis is the model scale test data obtained by Bousman (Ref. 19). The model was specifically designed to generate high

quality data over a wide rotor speed range and a series of different blade structural characteristics, and the data has been widely used for correlation and validation purposes (Refs. 17, 19).

The three-bladed rotor model is 5.5-ft. diameter, operating at tip speeds up to 275 ft/sec. The composite blades are very stiff in bending and torsion and are attached at the blade root with steel flap and lead-lag flexures of approximately 10% effective hinge offset. This arrangement effectively models an ideal rigid, hinged, spring-restrained blade configuration. For the test data used herein, no aeroelastic couplings were included. The fuselage is effectively a rigid body mass mounted on spring restrained gimbals for the pitch and roll degrees of freedom. The very low blade structural (0.65%) and gimbal friction damping of the model insured that the aeroelastic effects were not obscured by large nonlinear damping in the model. For the test data used herein, the rotor was operated over a wide range of rotor speeds at two collective pitch angles, 0° and 9°.

2GCHAS Analysis

2GCHAS structural model for this analysis consists of rotor and body subsystems. The body subsystem includes a rigid body mass, the two pitch and roll springs, and a stiff nonlinear beam element representing the shaft. The body was rigidly attached to the ground except for pitch and roll rotations. The rotor subsystem consists of three primitive structures, each representing a blade. Each blade includes three nonlinear beam elements, two lag and flap springs. The most inboard element is 3.35 in. long and connects the flap and lead-lag hinges to the hub. The second element is 12.2 in. long, the most outboard element is 16.32 in.. long, and together they model the blade. Uniform inflow was used for induced velocity model and linear unsteady airloads and momentum theory uniform inflow were used in the aerodynamic model. To generate the frequency and damping results, a linearized stability analysis was performed for a specified RPM range.

Correlation Results

Results are presented in two figures. The first results, Fig. 6, show the frequencies and damping for zero collective pitch for the full rotor speed range. The body pitch and roll modes, as well as the blade lead-lag regressing mode, are predicted accurately by the analysis, indicating that the basic dynamic coupling between flap, lead-lag, and body motions is validated. For the regressing lead-lag mode damping at zero pitch angle the analysis predicts the basic reduction in damping due to frequency coalescence, as confirmed by the experimental data. Similar results for damping are shown in Fig. 7 for a pitch angle of 9 degrees. There are differences in the level of the unstable damping and this is to be expected, since an unsteady wake (or dynamic inflow) model was not used for these calculations. Later correlations will use the Peters-He generalized dynamic wake. In view of these considerations, the 2GCHAS results fully confirm the validity of the basic structural and aeroelastic modeling for aeromechanical stability analysis.

Finite-Span Oscillating Wing Dynamic Stall

Dynamic stall is one of the most important aerodynamic phenomena influencing rotor blade loads and flight control system loads at high thrust levels and in high speed forward flight. It induces negative aerodynamic damping in torsion as well as stall delay. In some cases it may lead to stall flutter or torsional instability. Because of the complexity of the nonlinear unsteady aerodynamic phenomena associated with dynamic stall, most analytical methods are based on empirical approaches. The success or rotor loads prediction depends on the accuracy of such models. The 2GCHAS dynamic stall model (Ref. 1) is based on the work of Leishman-Beddoes and the combined airfoil wake modeling for a finite span wing configuration will be assessed by comparison with recently obtained experimental data. Piziali (Ref. 20) recently obtained excellent dynamic stall data suitable for validation of 3-D unsteady aerodynamic models. The model was a semi-span wing tested in the US Army Aeroflightdynamics Directorate (AFDD) 7- by 10- ft wind tunnel. The wing structure is a stiff uniform beam , and has a span of 5 ft, a chord of 1 ft, and NACA 0015 airfoil section. The inboard of the wing was attached to the wind tunnel wall. The testing consisted of oscillating the wing at various mean and oscillatory angles of attack and reduced frequency. Dynamic stall condition ranged from unstalled to deep stall cases. The effect of 3-D unsteady wake effects on airloads was well demonstrated. The data obtained included 2-D and 3-D dynamic stall as well as quasi-steady aerodynamics data.

2GCHAS Analysis

For the analysis, 2GCHAS employed one stiff nonlinear beam element coupled with ten aerosegments. Since the wing was attached to the wall, the analysis wing model had twice the actual beam length (10 ft), so that the half of the wing corresponded to the test model and had appropriate lift distribution. Leishman-Beddoes [1] unsteady aerodynamics model was used for aerodynamics, coupled with classical prescribed wake analysis. This unsteady aerodynamics model consists of calculation of an attached (potential) flow solution for the unsteady (linear) airloads, a separated flow solution for the nonlinear airloads, and a dynamic stall solution for vortex induced airloads. It also includes the shed wake effect by means of Wagner-like function. Since the shed wake effect was included by Leishman-Beddoes unsteady aerodynamics model, the Classical Prescribed Wake model involved only the trailing wake model. To obtain airloads, nonlinear transient response analysis was performed.

Correlation Results

Figure 8a-c shows the predicted lift and pitching moment coefficients correlation with the test data for the test conditions of 332.1 ft/sec (Mach number = 0.290, Reynolds number = 1.9532×10^6), a mean angle of attack of 13° with a 4° oscillating amplitude at a reduced frequency of 0.039. Near the wing tip, there is more downwash generated due to the tip vortex, reducing the angle of attack and stall. Correspondingly, the inboard locations experience more stall than the outboard span locations. As shown in Fig. 8a, the 47.5% span location experiences deep stall. After the onset of stall at an angle of attack of about 14°, the vortex tends to move toward the trailing edge, which delays lift stall and the pitching moment becomes slightly negative due to aerodynamic center shift. The vortex travels substantially toward the trailing edge and its strength decayed, and a large decay of the lift and a large negative pitching moment result. During the boundary layer reattachment, the separated flow tends to be normal, and the lift and pitching moment return to levels before the stall.

The Leishman-Beddoes unsteady aerodynamics model used in 2GCHAS, appears to do a good job predicting the stall phenomenon. As expected, the 80% span location experiences light stall, and, as shown in Fig. 8b, the prediction of the lift and the pitching moment seem reasonable. Similar trends are shown in Fig. 8c for the 90% span location although there is a slight overprediction of the pitching moment due to a lack of a tip vortex model. The 2GCHAS analysis predicts the 3-D dynamic stall behavior reasonably well, although a better wake model may improve the predictions near the tip of the wing.

S-76 Rotor Performance in 80- by 120-ft Wind Tunnel

Reference 21 recently presented S-76 performance data in hover and forward flight, tested in the NASA Ames 80- by 120-ft wind tunnel. This test established a data base of rotor performance and loads for the 0 to 100 knots airspeed with variation of shaft angles and thrust conditions. The objective of the test were to evaluate the capability of the 80- by 120-ft test section as a hover facility, to acquire forward flight rotor performance data. It was concluded that the hover performance data appeared slightly higher than would have been in free air, which apparently was caused by the facility wall effects.

The experiment was conducted using a full scale, production S-76 four-bladed rotor system of solidity 0.0748. The rotor was operated at 293 RPM with a tip speed of 675 ft/sec. The blade was 22 ft long with 3.5%, coincident flap-lag hinge offsets, and had 30° of tip sweep and -10° linear twist. The blade consisted of different cambered airfoil sections; SC-1095 outboard, SC-1095 R8 near 75% span, and SC-10XXR8 inboard. The rotor was mounted on the NASA modified Rotor Test Apparatus (RTA) which placed the rotor hub one rotor diameter above from the wind tunnel floor.

2GCHAS Analysis

For the performance analysis, the four-bladed, articulated rotor was modeled using single blade analysis. The blade was represented by seven nonlinear beam elements and seven aerodynamic segments. Nonlinear aerodynamics (table look-up) coupled with uniform inflow and an empirical factor of 1.10 (ratio of the induced power to ideal power) was used. The blade sweep was modeled such that the aerodynamic segments were aligned with the swept blade elastic axis while the blade structure was straight. (Alternatively, 2GCHAS could model the swept blade by sweeping the blade structure as

well as the aerodynamic segment.) The performance test data was limited to the hover case for the purposes of this correlation.

Correlation Results

S-76 rotor hover performance correlation is presented. The power coefficients (C_P/σ) are correlated in Fig. 9 with respect to the thrust coefficients (C_T/σ) over a range from low to high thrust levels. The results presented represent test data obtained from two different test configurations; one (0°) for the case that the fuselage is aligned with the tunnel center line and facing the tunnel inlet and the second (90°) with the fuselage yawed 90 degrees clockwise. For low thrust level, the two test data are quite close to each other and seem reliable, and they are also in good agreement with the 2GCHAS prediction. At higher thrust levels, where there are larger differences between the two test data, the predicted results were between two sets of test data. The majority of the discrepancy in the test data was concluded in Ref. 21 to be due to the facility effect. With the thrust level, the same trend appears for the figure of merit as for C_P/σ.

For the full scale S-76 performance data, 2GCHAS demonstrated good prediction capability in the low thrust level, and it seems sufficiently accurate even for high thrust level ($C_T/\sigma = .1$) considering the discrepancy of the test data.

CH-47C Model Rotor Blade Airloads

A major obstacle to the understanding of the dynamic stall phenomenon, apart from the complexity of the phenomenon itself, is the lack of good test data. Reference 22 presents one of the few dynamic stall data sets which is particularly valuable for engineering validation. The model was a CH-47C rotor having fully articulated, 1/7.5 scale blades, and it was tested in the 20- by 20-ft Boeing Vertol Wind Tunnel. The data is available for two flight conditions. At CT/σ of 0.105 and 0.132 with advance ratio of 0.35 (tip speed of 500 ft/sec), the experimental data of aerodynamic coefficients without drag at 75% blade location is described in the reference.

2GCHAS Analysis

For the analysis, the rotor blade was modeled by one stiff nonlinear beam element with ten aero segments. For the aerodynamics, Leishman-Beddoes unsteady aerodynamics and classical prescribed wake models were used to include the 3-D unsteady aerodynamics effect. To obtain airloads, nonlinear transient response analysis was performed.

Correlation Results

Time history of normal force coefficient at CT/σ of 0.105 with advance ratio of 0.35 in the 75% blade location, is shown in Fig. 10. The symbol represents the test data, and the solid line is for 2GCHAS. The test data shows deep stall, and the vortex induced lift in the retreating side is well predicted by 2GCHAS. During the process of reattachment (azimuth angle near 360 degrees), the boundary layer separation point tends to move from the leading edge to the trailing edge so quickly. This may cause oscillation of normal force as shown in the test data, and 2GCHAS prediction of the trend for normal force coefficient during the reattachment process seems quite reasonable. The corresponding pitching moment coefficient is also given in Fig. 10. After initiation of stall, the vortex begins to propagate toward the trailing edge. The vortex induced lift becomes larger (stall delay), and also the center of pressure shifts from the aerodynamic center toward the trailing edge, which results in large negative pitching moment. As the vortex lift decays due to full separated flow development, the (negative) pitching moment becomes smaller, though the center of pressure is near the mid-chord. After a while, the boundary layer begins to be reattached and the separation point of the boundary layer tends to move toward the trailing edge. The pitching moment prediction modeled based on these complex physics of dynamic stall behavior, appears quite satisfactory. It is demonstrated that the 2GCHAS capability to predict rotor dynamic stall is quite satisfactory for current empirical methodology.

UH-60A Black Hawk Flight Test Airloads and Vibratory Loads

For the rotor model, the rotorcraft vibratory loads has been regarded as one of the most difficult tasks to predict. Since it integrates influence of structure, aerodynamics, and controls, the source of discrepancy of correlations cannot be easily identified. The vibratory loads transmit to the fuselage, and determine the aircraft vibration level. Ref. 23 addressed the status of understanding rotorcraft vibratory loads prediction to this day by

presenting vibratory loads correlation for Puma and UH-60A Black Hawk (Phase 1) in free flight. It concluded that the qualitative prediction of the blade vibratory flap bending moments for UH-60A was less satisfactory, but quite good for the research Puma. Since there was, however, no pressure instrumentation installed for the UH-60A Phase 1 flight, the airloads data was not available. Correspondingly, justification of the discrepancy of vibratory loads prediction without airloads data was quite difficult. Recently, the airloads and vibratory loads of NASA/Army UH-60A Airloads Program Phase 2 flight test data has become available (Ref. 24). Though the flight test data used herein must be considered preliminary, the extent and scope of this data mean that it will be an extremely valuable resource for the development and refinement of rotorcraft prediction methods and was considered suitable for the present initial engineering validation.

The UH-60A Black Hawk Phase 1 flight test data (Flt. 9) were obtained during a NASA/Army test in 1987. The aircraft had a production version, four-bladed, articulated main rotor and single tail rotor. The main rotor blade was instrumented with four flap bending moment bridges. There was, however, no pressurized instrumentation installed. Approximately, five seconds of data were obtained at each test data point, and the bandwidth of 128 harmonics were extracted. The test data ranged from advance ratio of 0.1 to 0.355. and were well distributed within the flight speed range. Recently, new flight test data (Flt. 85) of the same UH-60A aircraft (Phase 2) became available (Ref. 24). This Phase 2 data included pressure data as well as vibratory loads. It contained quite useful airloads data in addition to vibratory loads, although this aircraft (Flt. 85) did not fly in the medium speed range.

The main rotor was operating at the values of about 260 RPM with a tip speed of about 725 ft/sec. The solidity was 0.08317. The blade was 26.833 ft long with 4.66%, coincident flap-lag hinge offsets, and had 20° tip sweep and -16° linear twist. The blade consisted of different cambered airfoil sections; SC-1095 outboard, SC-1095 R8 near 75% span and again SC-1095 inboard.

2GCHAS Analysis

Figure 11 shows the geometry of the UH-60A production blade. The blade has high twist distribution (-16°), 20 degrees of sweep outboard of the 91% blade span, and consists of SC-1095 and SC-1094R8 airfoil sections. For the analysis, the fully articulated main rotor was modeled by four blades. Each blade was identical, discretized into six nonlinear beam elements and ten aerodynamic segments. Determination of the boundary of each beam element or aerodynamic segment was primarily based on accuracy of the solution and numerical efficiency, but also depended on the consideration of the blade span locations of the flight test data in order to correlate with more span locations.

Several different airloads models (simple, nonlinear, and unsteady) and various wake models (uniform inflow, prescribed wake, free wake, and Wagner-like function shed wake) were varied to investigate how the models influence vibratory loads and blade section airloads. The free wake model used in the analysis was a single peak model. This single peak free wake model improved the vibratory loads correlation significantly, compared with the dual peak model which was used in Ref. 23. The wake aging angle was 60 azimuthal degrees for the near wake, 60 degrees for the wake roll-up, three rotor revolutions for the far wake and tip vortices. The age of each wake element was 15 degrees. The core radii of tip vortices for on-blade velocity were 9.2% of the blade radius, and those for interference velocity were 3.2%. The inboard trailed, shed, roll-up, and near wake core radii were from the default values. The blade sweep was modeled such that the aerodynamic segments were aligned with the swept blade elastic axis while the blade structure was straight. To obtain the airloads and loads (bending moments), the nonlinear system equations were iterated by a time integration under the rotors-body, fully coupled trim conditions until the converged solution was obtained. The harmonics of loads (vibratory loads) were postprocessed by 2GCHAS output processor.

Blade Frequency Correlation Results

In order to validate the structural model, the natural frequencies (in vacuum) of the UH-60A production blade are calculated and compared in Fig. 12 between 2GCHAS and CAMRAD/JA. The first three flap, two lead-lag, and one torsion modes are presented with RPM sweep. The third flap, second lead-lag, and first torsion modes appeared strongly coupled (frequency coalescence) between 60 - 80% nominal rotor speed. For higher modes, the

predictions by the two analyses are shown to be slightly different from each other due to different structural nonlinear models. For the nonrotating frequency calculation, 2GCHAS well demonstrated consistency of the frequency prediction, while CAMRAD/JA showed some discontinuity of the modal frequencies. However, overall the two analyses are in good agreement.

Phase 1 Blade Loads Results

Figure 13 shows the comparison of the calculated 3/rev vibratory flap moments at the mid span using 2GCHAS and CAMRAD/JA with the UH-60A Black Hawk Phase 1 flight test data (Flt. 9). The 2GCHAS analysis included Leishman-Beddoes unsteady aerodynamics model with free wake single-peak option. The shed wake effect was included by the Wagner-like function implemented in the Leishman-Beddoes unsteady aerodynamics model. For CAMRAD/JA, the analysis options were set up to be virtually the same as in 2GCHAS, and they included nonlinear aerodynamics (table look-up) with static stall and linear unsteady aerodynamics effects, and, the free wake single-peak model with trailed, shed, tip vortex, roll-up, and near wake effects was used. As shown in Fig. 13, both of the analyses generally give good prediction of the 3 per rev flap moment in the low speeds, but substantial difference in the high speeds, although the 2GCHAS analysis shows a spike near an advance ratio of 0.2. The prediction of the phase of 3 per rev flap moment by both of analyses appears quite satisfactory, as shown in Fig. 13.

To investigate the different aerodynamics effects, the nonlinear aerodynamics and uniform inflow models are considered for the 2GCHAS analysis. Fig. 14 shows the 3 per rev flap bending moment comparison with the flight data. For the nonlinear aerodynamics model with uniform inflow, the bending moment prediction appears to be very low for the low speed, but it improves as the flight speed increases. For nonlinear aerodynamics with a free wake, the prediction improve considerably compared with the uniform inflow case, but it is less as good as the case with the Leishman-Beddoes unsteady aerodynamics model with a free wake. For the flap moment predictions, the analysis with the Leishman-Beddoes unsteady aerodynamics model coupled with a free wake is better than the other two cases.

Phase 2 Blade Loads and Airloads

The UH-60A Phase 2 flight test data (Flt. 85), which recently became available, supplies the data of airloads as well as the blade moments, while Phase 1 data includes the blade moments only. It is noted that this Phase 2 data (Flight 85) covers the data in the low and high speed flights, and the flight test for the medium speed range are not conducted. The airloads are compared with the UH-60A Phase 2 flight test data (Flt. 85) for two airspeeds (advance ratios of 0.105 and 0.368) by using 2GCHAS and CAMRAD/JA. For comparison, the lift and pitching moments in three blade span locations (r/R=0.55, 0.775, 0.965) are considered. Figure 15 presents the comparison of lift at an advance ratio of 0.105. The 2GCHAS analysis model used for this study was set virtually equivalent to that of CAMRAD/JA, except that 2GCHAS employed the Leishman-Beddoes unsteady aerodynamics model including shed wake effects while CAMRAD/JA included nonlinear aerodynamics (table look-ups with stall correction) with the free wake shed wake effect. The trimmed values for the angles of attack in these span locations ranged from -1.3 to 7.9 degrees. The analyses by 2GCHAS as well as CAMRAD/JA substantially overpredict the lift peak-to-peak values of the flight data shown in three span locations for the first half of the rotor revolution, while they are in good agreement for the second half of the rotor revolution. For the first half rotor revolution, the 2GCHAS prediction of the waveform shows some time lag of the lift for the inboard stations, and is improved in the outboard stations. The CAMRAD/JA prediction for the first half is somewhat better, but still unsatisfactory. This discrepancy in the first half may be caused partially by the linear unsteady aerodynamics model. For the pitching moment, the both analyses substantially over predict for the 77.5% span, but appear satisfactory for the 96.5% span. The test data shows evidence of possible measurement error, that becomes more significant for the outboard portion of the blade. The 2GCHAS analysis captures well higher harmonics of the waveform especially for the 96.5% span, while the CAMRAD/JA prediction is shown by the quite smooth representation. Note that the flight test data at the 55% span location contains lots of noise, and so is removed from the comparison.

For high advance ratio of 0.368, the lift correlations are given in Fig. 16. Under this flight condition, it was difficult to obtain a trim solution, and both

analyses experienced difficulties in obtaining converged numerical solutions at the prescribed wake level. For 2GCHAS, the solution did not converge during Newton-Raphson time integration with the Leishman-Beddoes unsteady aerodynamics model. The converged solution results presented were achieved with a nonlinear aerodynamics (table look-up) model including the shed wake in the free wake model instead of the Leishman-Beddoes unsteady aerodynamics. For CAMRAD/JA, the solution by the harmonic balance method was reasonable even though the output warned that the trim solution was not converged, and these results are presented. The lift predictions along the blade span by 2GCHAS as well as CAMRAD/JA show some discrepancies for the first half of the rotor revolution and are satisfactory for the second half. As shown in the low speed case (Fig. 15), the 2GCHAS lift prediction at the 55% blade span gives a large discrepancy.

In order to identify possible causes of differences between the two analyses, results were obtained for a simple rotor case were made for 2GCHAS as well as CAMRAD/JA. A torsionally stiff UH-60A blade was used with a basic linear airfoil aerodynamics model with uniform inflow. For both 2GCHAS and CAMRAD/JA, nearly identical aerodynamics coefficients were obtained, except for the 55% span lift coefficient in 2GCHAS. The lift coefficient and angle of attack at this span location were not completely consistent with each other, but this discrepancy is considered a minor problem in 2GCHAS. It was also not possible to get uniformly distributed inflow along the azimuth in CAMRAD/JA, because of the increment of nonuniform inflow due to rotor pitching and rolling moments not controllable by the user input. However, results from this simple model were sufficient to confirm the aerodynamic coefficients between two analyses to be quite close to each other.

The pitching moments using 2GCHAS and CAMRAD/JA are compared in Fig. 16 with the flight test data with an advance ratio of 0.368. The predictions by two analyses are generally close to each other, and show some discrepancies compared with the flight data, and these discrepancies are inconsistent. For the 55% span location, the mean value of the negative pitching moment from the analyses is slightly low compared with the test data, and the waveform predictions are generally good. The predictions of the negative pitching moment for the 77.5% span appear substantially high in the first half of the rotor revolution, while the second half look quite satisfactory. The flight test data of pitching moment for the 96.5% span is oscillating in the first half of the rotor revolution, but those in the analyses are smooth. In the second half, the analyses are slightly underpredicting the negative pitching moment. Though it is difficult to summarize the airloads correlations in this preliminary study, the predictions of the lift and pitching moment by two analyses generally show discrepancy in the first half of the rotor revolution and quite satisfactory in the second half. It certainly requires further investigation to understand and identify the source of the discrepancy in the near future.

Phase 2 Airloads Sensitivity Investigation

A limited investigation for the discrepancies between the analyses and the test data was conducted using different aerodynamic options. Figure 17 shows the lift comparisons in the 55% span location for an advance ratio of 0.105 using the 2GCHAS analysis. The 2GCHAS analysis results include: 1) the Leishman-Beddoes unsteady aerodynamic model having a free wake and the Wagner-like function shed wake options, 2) the nonlinear aerodynamics model having a free wake option including the shed wake effect, but without the linear unsteady aerodynamics effect, and 3) the Leishman-Beddoes unsteady aerodynamics with uniform inflow. The first two results with a free wake option are similar and show large oscillations in the first half compared with the flight data. The analysis with the Leishman-Beddoes model improves the correlation slightly compared to that with the nonlinear aerodynamics, and this may be due to linear unsteady aerodynamics effect. The analysis with the Leishman-Beddoes unsteady aerodynamics coupled with a uniform inflow option appears quite close to the flight data, except that it does not have harmonic variations due to a simple wake model. This is quite interesting, but the reason is not well understood yet.

Similarly, different options were exercised using the CAMRAD/JA analysis. For an advance ratio of 0.105, the lift in the 55% blade span is compared with the flight test data in Fig. 18. The CAMRAD/JA analyses include: 1) a free wake model with (linear) unsteady, aerodynamic yaw, and radial drag effects, 2) no yaw and no radial drag effects, and 3) no unsteady aerodynamic effect. The first two results are quite close to each other, and the aerodynamic yaw and radial drag effects seem quite

small. The curve without the unsteady aerodynamic effect shows a substantial oscillation in the lift compared with the flight data. This large oscillation behavior was evident in the 2GCHAS results but the unsteady aerodynamic effect in was not significant (Fig. 17). It may be concluded, therefore, that the unsteady aerodynamics plays a significant role in the airloads correlation, and the unsteady aerodynamics model used in 2GCHAS may need further investigation and refinement.

Phase 2 Blade Loads Correlation Results

The blade bending moments of the UH-60A phase 2 flight test are correlated. For two air speeds (advance ratios of 0.105 and 0.368), the flap and chord bending moments and the torsional moments are compared using the 2GCHAS and CAMRAD/JA analyses. The flight test data are described by up to 124 harmonics, and the time history of the blade moments were generated by means of the harmonics analysis. During this process, the mean value was taken out because the mean values from the two analyses were significantly different from the flight data. Figure 19 shows 1-124 P (per rev) flap bending moments in the 11.3%, 50.0%, and 90.0% span locations for an advance ratio of 0.105. For the 11.3% span, two analyses predict the moment reasonable, except for the scattering of the flight data. The peak-to-peak value of the moment by 2GCHAS is substantially high, while that by CAMRAD/JA appears reasonable. The cause of this discrepancy is not yet known and is under investigation. For the 90% span, two analyses well predict the moment, and CAMRAD/JA appears better in the first quadrant of the rotor revolution and 2GCHAS seems better in the second quadrant. For the lead-lag bending moment, the comparison of two analyses with the flight test data for an advance ratio of 0.105 is shown in Figure 19 Compared with the flight data, the 2GCHAS analysis predicts the moment obviously better than the CAMRAD/JA for the 11.3% and 90% span, although both of the analyses show substantial discrepancies. Figure 19 also shows the comparison of the torsional moment in the 90% span. The 2GCHAS results generally overpredict the moment especially in the advancing side and show significant discrepancy compared with the flight data. The CAMRAD/JA results show significant phase lag and substantial error in the fourth quadrant of the rotor, the same as in the 2GCHAS results.

For an advance ratio of 0.368, the flap bending moments are compared in Fig. 20. For the 2GCHAS analysis, the nonlinear aerodynamics model having free wake option was employed since it was not able to get the converged trim solution with the Leishman-Beddoes unsteady aerodynamics model having free wake option but without the linear unsteady aerodynamics. Because of lack of the linear unsteady aerodynamics effect, the analysis shows slightly high oscillation of the lift in the first half of the rotor and is expected to have substantially high oscillation in the first half for the high speed, where the unsteady aerodynamics effects are substantially important. Due in part to this reason , the flap moments predicted by 2GCHAS for the 11.3%, 50.0%, and 90.0% spans show substantial oscillations, while the CAMRAD/JA shows the similar trend as for the low speed case. For the lead-lag bending moments for the 11.3% and 50.0% spans, both of the analyses predictions show substantial discrepancies, the trends are similar as shown for the low speed case, and the 2GCHAS analysis prediction is slightly better than the CAMRAD/JA analysis. For the torsional moment in the 90.0% span, the 2GCHAS analysis prediction is slightly better than the CAMRAD/JA, unlike in the low speed case, even though both of the analyses display substantial discrepancyies These blade moment calculations are integrals of the structure, aerodynamics, and controls. There are shown some inconsistent trends between the low and high flight speeds. The trends shown in the airloads and blade moments are not consistent. Though it is difficult to summarize the conclusion of the correlations, it is certainly clear that there is a strong need for further investigation to identify the source of the discrepancy in the near future.

Conclusions

Correlation of 2GCHAS with experimental results was conducted for a wide range of rotorcraft aeromechanics characteristics. The correlations must be regarded as preliminary in some respects, since not all of the capabilities of the System were exercised. However, for a comprehensive analysis, one of the objectives is to demonstrate that the basic aerodynamics and dynamics formulation is valid for a wide range of applications. It may be concluded on the basis of the present results that within the scope of the experimental data employed, 2GCHAS provided very satisfactory results. In some areas, agreement with test data was not acceptable, in

some cases due to the preliminary nature of the test data or known experimental uncertainties. In other cases the analysis was likely responsible for the discrepancies and these will be addressed in future work.

To summarize the key findings in the individual areas of correlation, the following additional comments are made:

1. The 2GCHAS nonlinear beam element is satisfactory within the range of moderate deformations. A desireable improvement would be to remove the limitations of the large angle kinematics from the present formulation.

2. The torsionally soft hingeless rotor aeroelastic stability correlation further confirms the basic structural capabilities of the nonlinear beam element, but the differences found may warrant additional investigation. Use of the 2GCHAS generalized dynamic wake is expected to improve the correlation.

3. The basic features of hingeless rotor aeromechanical stability were successfully predicted by 2GCHAS. More general configurations, including bearingless rotors, will be used to further validate the System.

4. For the 3-D finite span dynamic stall case, 2GCHAS analysis satisfactorily predicts 3-D stall behavior, and the use of better wake model may improve the correlation for the outboard span.

5. For the full scale S-76 performance data, 2GCHAS demonstrated good prediction capability at low thrust level, and it seems sufficiently accurate even in the high thrust level considering the departure of the test data from a true hover condition. Further correlations will be made with other test data.

6. From the CH-47C model rotor blade airloads correlation, the basic 2GCHAS capability for rotor dynamic stall prediction on lifting rotor blades was confirmed and appeared quite satisfactory.

7. For the UH-60A Black Hawk Phase 1 flight test, prediction of the magnitude of the 3 per rev vibratory loads by 2GCHAS was reasonable in the low speed, and not satisfactory for medium and high speeds, while the CAMRAD/JA predictions were satisfactory except at high speed. The phase prediction was quite good for both analyses. The Leishman-Beddoes unsteady aerodynamics model with a free wake gave the best results.

8. For the UH-60A Black Hawk Phase 2 flight test, the 2GCHAS and CAMRAD/JA analyses show substantial discrepancies for prediction of airloads as well as blade moments. Unsteady aerodynamics probably has a major impact on airloads as well as blade moment. These correlations are, however, preliminary, and there is a strong need for further investigation to identify the source of the discrepancy in the near future.

Acknowledgments

The authors would like to thank Dr. R. A. Ormiston, AFDD for invaluable comments and advice toward completion of the paper, and Dr. M. J. Rutkowski and Dr. G. C. Ruzicka, AFDD for help to complete this paper, and also give many thanks to Mr. T. H. Maier and Mr. W. G. Bousman, AFDD for the UH-60A flight test data and CAMRAD/JA data.

References

1. Anon. 2GCHAS Theory Manual, Vols. I and II, U.S. Army Aeroflightdynamics Directorate (ATCOM), November 1993.

2. Anon. 2GCHAS User's Manual, Vols. I and II, U.S. Army Aeroflightdynamics Directorate (ATCOM), July 1993.

3. Anon. 2GCHAS Applications Manual, U.S. Army Aeroflightdynamics Directorate (ATCOM), July 1993.

4. Ormiston, Robert A., Ruzicka, Gene C., Tan, Carina M., and Rutkowski, Michael J., "First Level Release of 2GCHAS for Comprehensive Helicopter Analysis," Paper presented at the Seventeenth European Rotorcraft Forum, Berlin, Germany, September 24-26, 1991.

5. Rutkowski, Michael J., Ruzicka, Gene C., Tan, Carina M., Ormiston, Robert A., and Stephens, Wendell B., "First Level Release of 2GCHAS for Comprehensive Helicopter Analysis – A Status Report," Paper presented at the AHS International Technical Specialists' Meeting on Rotorcraft Basic

Research, Georgia Institute of Technology, March 22-27, 1991.

6. Stephens, Wendell B.; Rutkowski, Michael J.; Ormiston, Robert A.; and Tan, Carina M., "Development of the Second Generation Comprehensive Helicopter Analysis System (2GCHAS)," Paper presented at the American Helicopter Society National Specialists' Meeting on Rotorcraft Dynamics, Arlington, Texas, November 13-14, 1989.

7. Kerr, Andrew W. and Davis, John M., "A System for Interdisciplinary Analysis -- A Key to Improved Rotorcraft Design," Presented at the 35th Annual Forum of the AHS, paper No. 79-8, Washington, D.C., May 1979.

8. Kerr, Andrew, W. and Stephens, Wendell B., "The Development of a System for the Interdisciplinary Analysis of Rotorcraft Flight Characteristics," AGARD Conference Proceedings on Prediction of Aerodynamic Loads on Rotorcraft, AGARD-CP-334, May 1982.

9. Stephens, Wendell B. and Austin, Edward E., "Comprehensive Rotorcraft Analysis Methods. NASA/Army Rotorcraft Technology," Volume I -- Aerodynamics, and Dynamics and Aeroelasticity, NASA CP 2495, 1988.

10. Ruzicka, Gene C., and Ormiston, R.A., "Fundamental Dynamics Issues for Comprehensive Rotorcraft Analyses," Paper presented at the American Helicopter Society National Specialists' Meeting on Rotorcraft Dynamics, Arlington, Texas, November 13-14, 1989.

11. Ruzicka, Gene C., and Ormiston, R.A., ``Finite-Element Analysis and Multibody Dynamics Issues in Rotorcraft Dynamic Analysis," Presented at the Seventeenth European Rotorcraft Forum, Berlin, Germany, September 24-26, 1991.

12. Hamilton, Brian K., Straub, F.K., and Ruzicka, G.C., ``A General Purpose Nonlinear Rigid Body Mass Finite Element for Application to Rotary Wing dynamics," Presented at the American Helicopter Society International Technical Specialists' Meeting on Rotorcraft Basic Research," Atlanta, Georgia, March, 1991.

13. Ormiston, Robert A., Rutkowski, Michael J., Ruzicka, Gene C., Saberi, Hossein, and Jung, Yoon, "Comprehensive Aeromechanics Analysis of Complex Rotorcraft Using 2GCHAS," Paper presented at the American Helicopter Society Aeromechanic Specialists Conference, San Francisco, California, January 19-21, 1994.

14. Hodges, D. H., Dowell, E.H., "Nonlinear Equations of Motion for the Elastic Bending and Torsion of Twisted Nonuniform Rotor Blades," NASA TN D-7818, Dec. 1974.

15. Dowell, E.H., and Traybar, J.J., ``An Experimental Study of the Nonlinear Stiffness of a Rotor Blade Undergoing Flap, Lag and Twist Deformations," AMS Report 1257, Department of Aerospace and Mechanical Sciences, Princeton University, Dec. 1975.

16. Sharpe, David L., "An Experimental Investigation of the Flap-Lag-Torsion Aeroelastic Stability of a Small-Scale Hingeless Helicopter Rotor in Hover," NASA TP 2546, AVSCOM TR 85-A-9, January 1986.

17. Sharpe, David L., "A Comparison of Theory and Experiment for Aeroelastic Stability of a Hingeless Rotor Model in Hover," Proceedings, Integrated Technology Rotor Assessment Workshop (1983), NASA CP 10007; AVSCOM CP 88-A-001, June 1988.

18. Andrade, D., and Peters, D.A., ``Correlation of Experimental Flap-Lag-Torsion Damping - A Case Study," 49th Annual Forum of AHS, St. Louis, MO, May 1993`.

19. Bousman, William G., "A Comparison of Theory and Experiment for Coupled Rotor-Body Stability of a Hingeless Rotor Model in Hover," Proceedings, Integrated Technology Rotor Assessment Workshop (1983), NASA CP 10007; AVSCOM CP 88-A-001, June 1988, pp. 43-65.

20. Piziali, R.A., ``An Experimental Investigation of 2D and 3D Oscillating Wing Aerodynamics

for a Range Angle of Attack Including Stall," NASA TM/ATCOM TR to be published.

21. Shinoda, P.M., and Johnson, W., ``Performance Results from a Test of an S-76 Rotor in the NASA Ames 80- bt 120-foot Wind Tunnel," AIAA 11th Applied Aerodynamics Conference, AIAA-93-3414, Monterey, CA, August 1993.

22. Fisher, Richard K., Jr., Tompkins, Jerome E., Bobo, Christopher J., and Child, Richard F., "An experimental Investigation of the Helicopter Rotor Blade Element Airloads on a Model Rotor in the Blade Stall Regime,"NASA CR-114424, Sept. 1971.

23. Bousman,W.G., and Maier, T.H., ``An Investigation of Helicopter Rotor Blade Flap Vibratory Loads," 48th Annual Forum of AHS, Washington,D.C., June 1992.

24. NASA/Army UH-60 Black Hawk Loads Program Final Report, to be published.

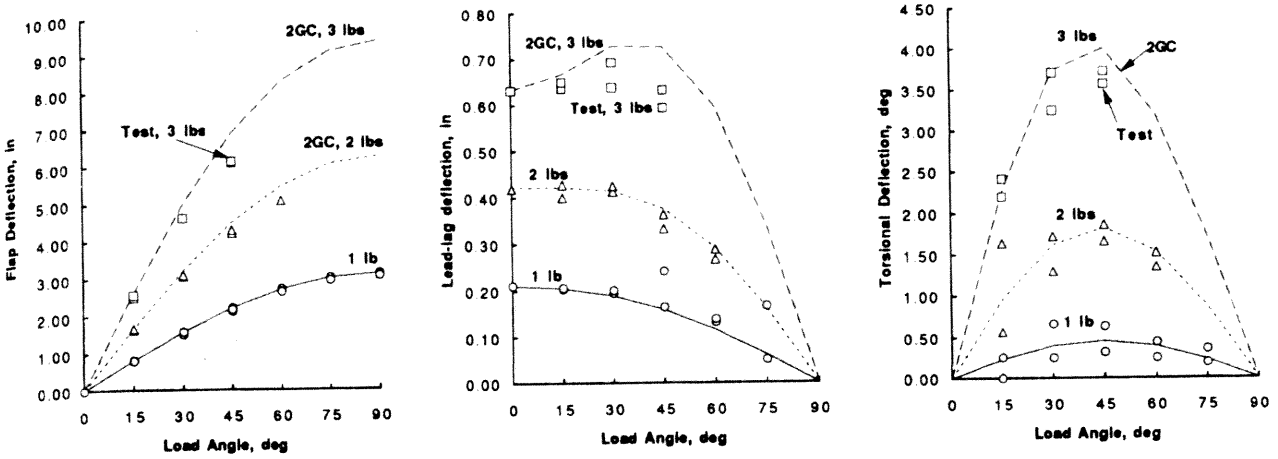

a) Varying load angle, upgraded nonlinear beam element.

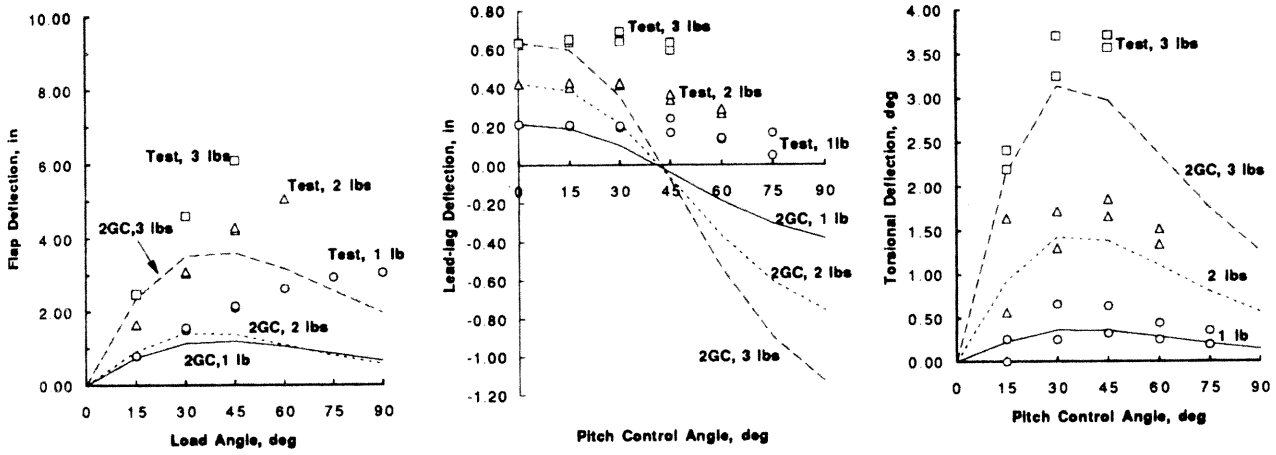

b) Varying pitch angle, original nonlinear beam element

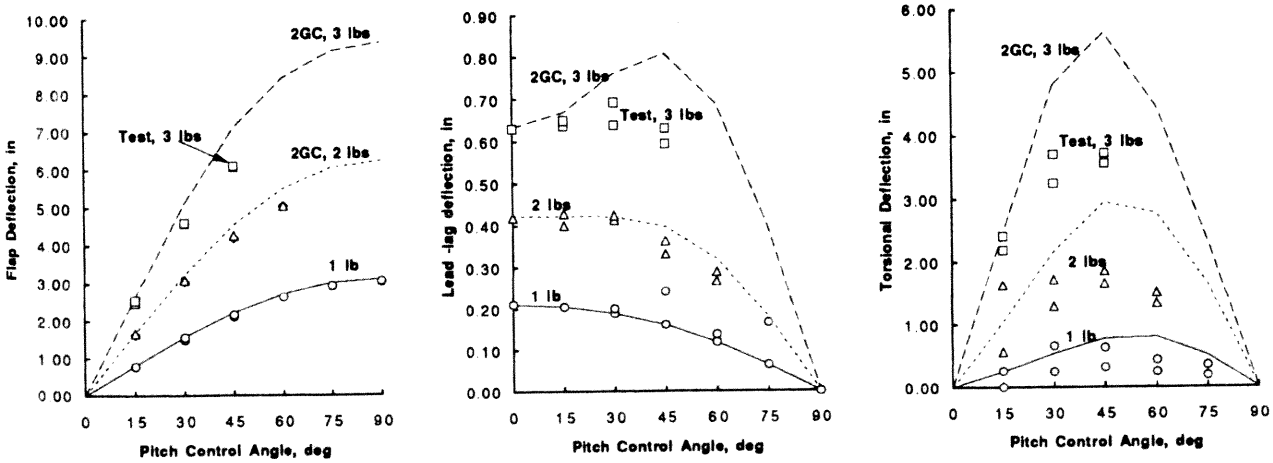

c) Varying pitch angle, upgraded nonlinear beam element.

Fig. 1. Nonlinear beam static structural bending and torsion deflections.

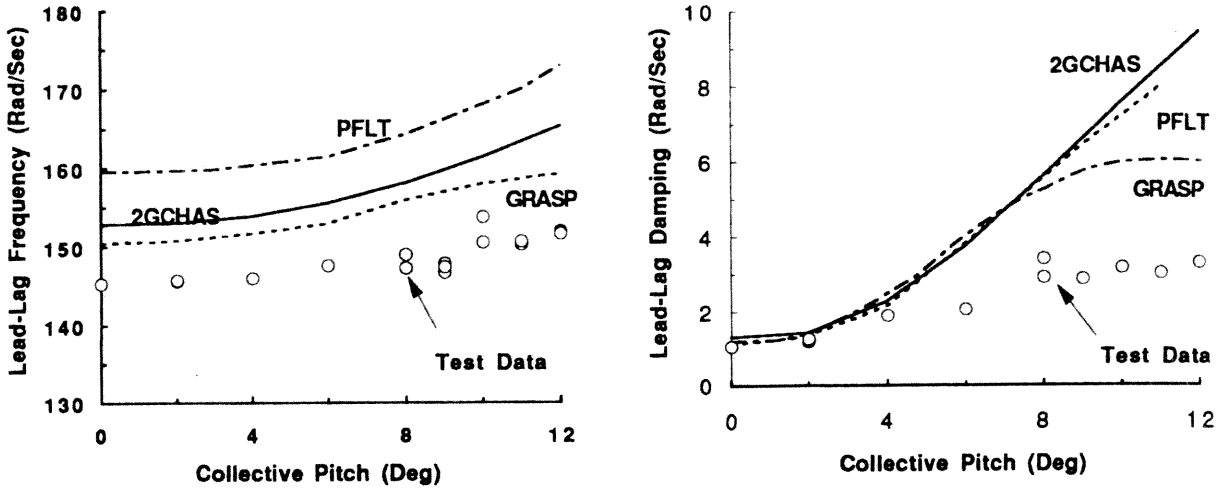

Fig. 2. Hingeless rotor blade aereolastic stability, frequency, and damping versus collective pitch, no precone or droop.

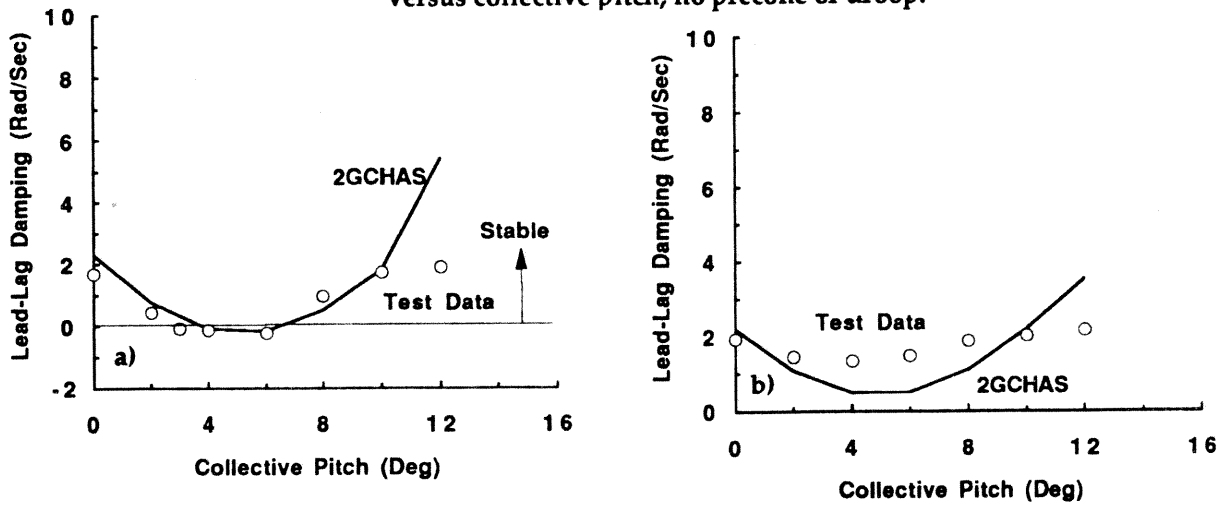

Fig. 3. Hingeless rotor blade damping versus collective pitch, 5° precone, a) Soft pitch flexure, b) Stiff pitch flexure

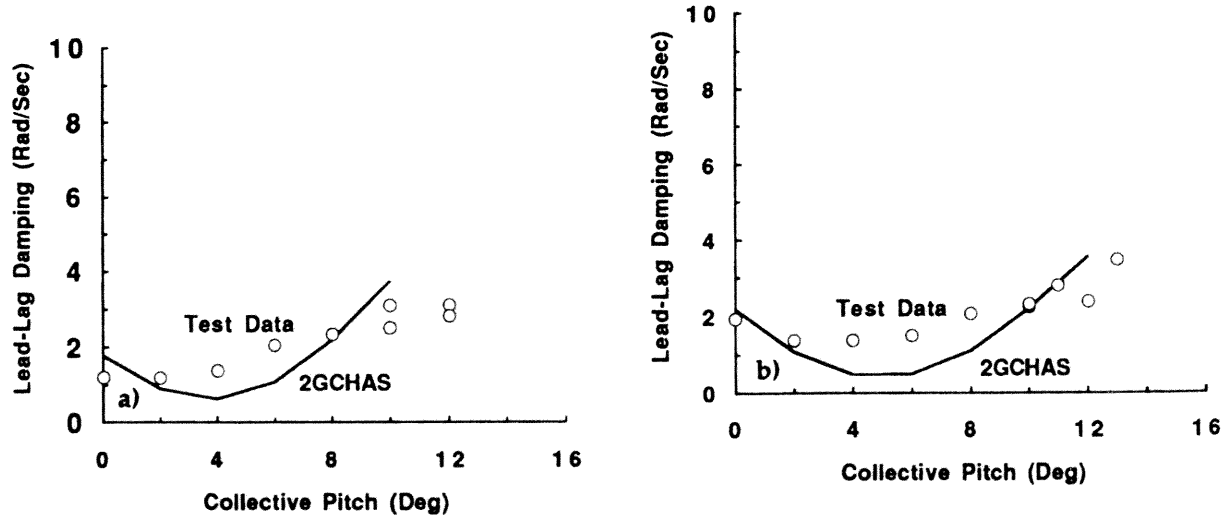

Fig. 4. Hingeless rotor blade damping versus collective pitch, 5° negative droop, a) soft pitch flexure, b) stiff pitch flexure.

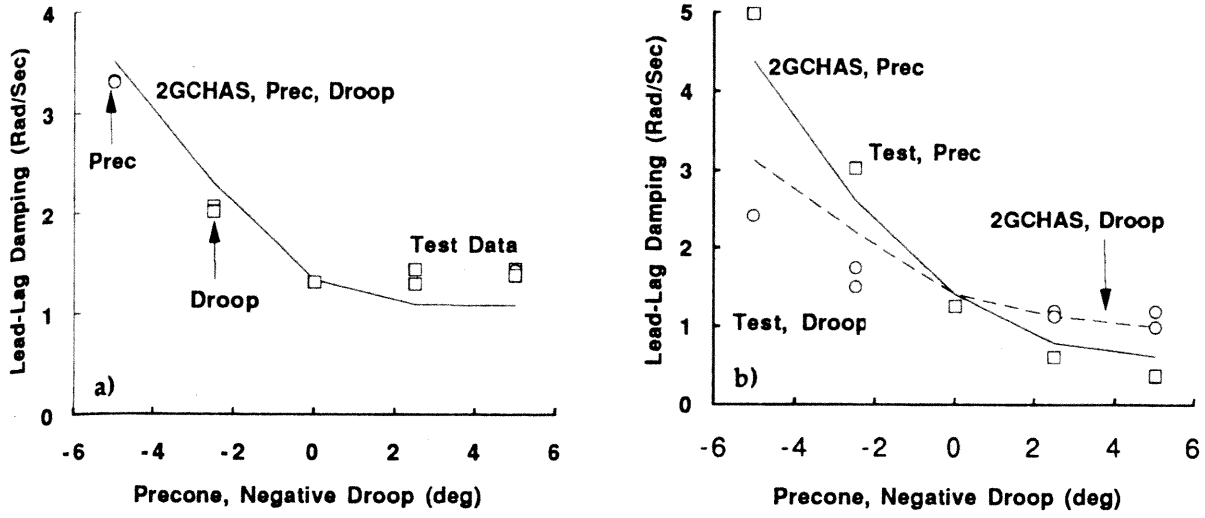

Fig. 5. Hingeless rotor blade damping versus precone and droop angle for 2 degrees collective pitch, a) stiff pitch flexure, b) soft pitch flexure.

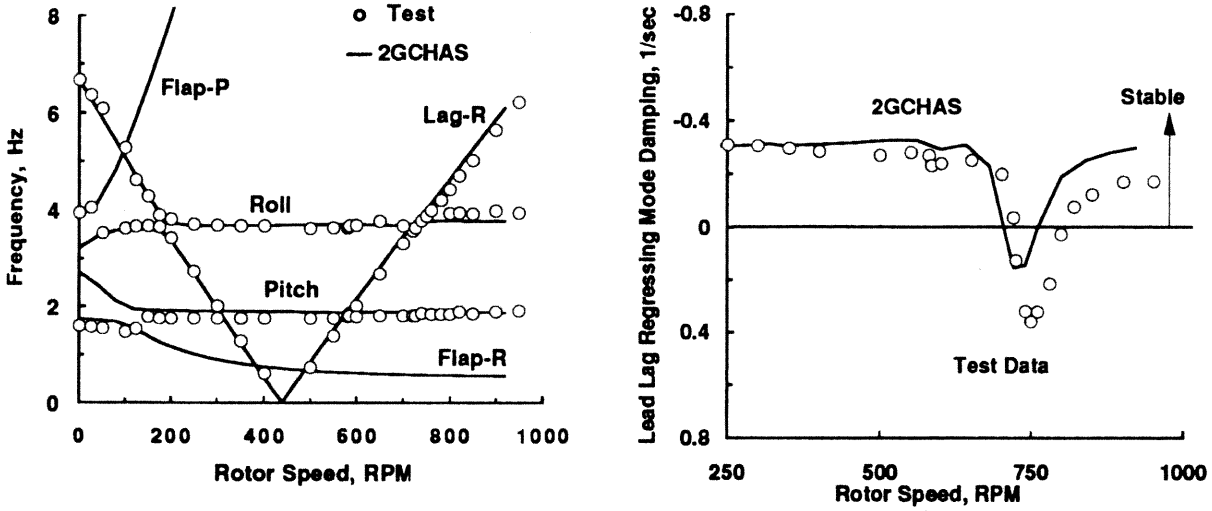

Fig. 6. Coupled hingeless rotor-body aeromechanical stability, frequency and damping, 0 deg collective pitch.

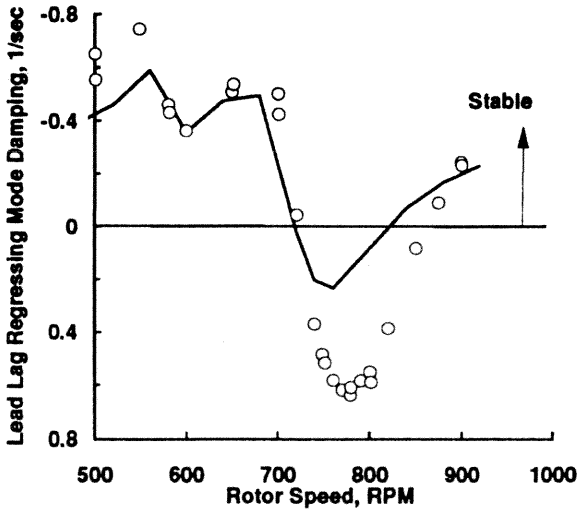

Fig. 7. Coupled hingeless rotor-body aeromechanical stability, damping, 9 deg collective pitch.

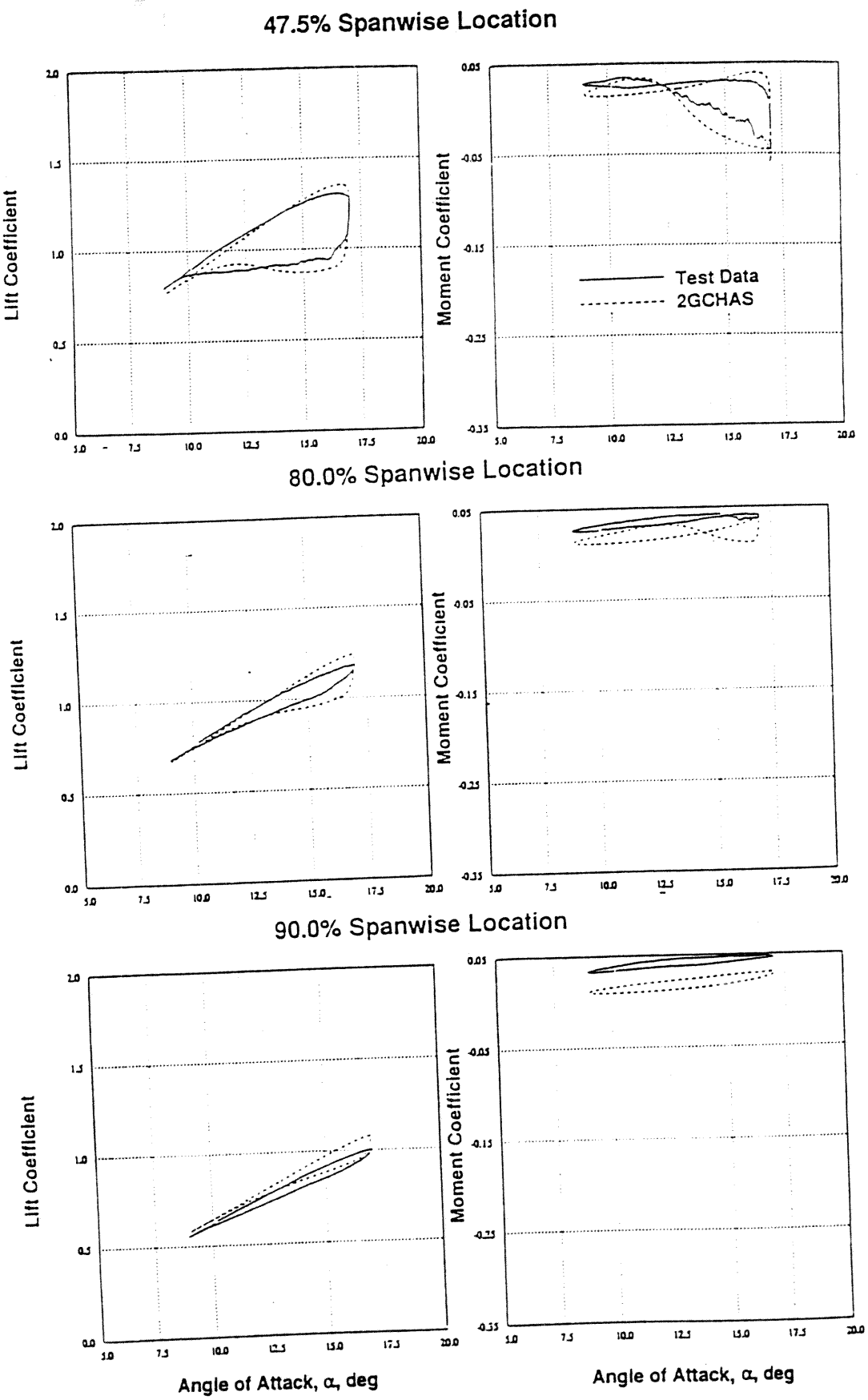

Fig. 8. Lift and moment coefficients versus angle of attack for 3D oscillating wing a) 47.5% span, b) 80% span, and c) 90% span

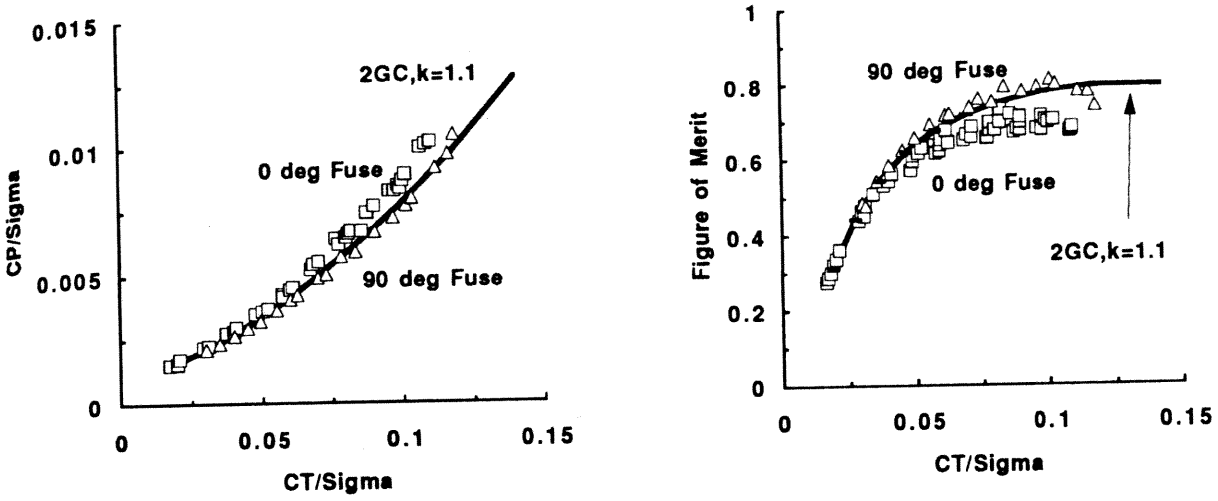

Fig. 9. Performance characteristics for S-76 rotor in 80- by 120-Ft Wind Tunnel.

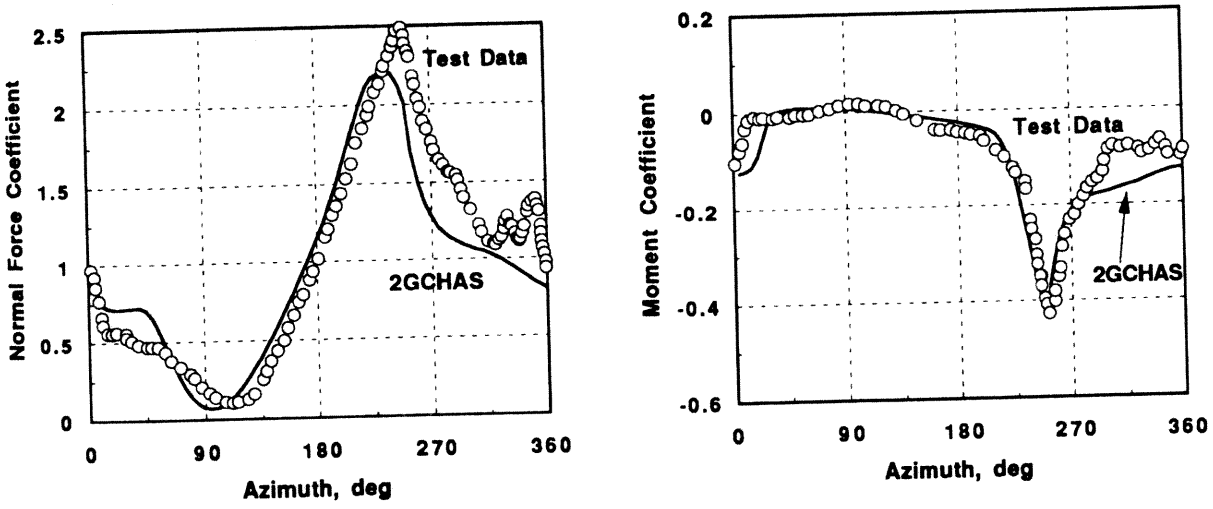

Fig. 10. Rotor blade normal force and moment airloads versus azimuth for a CH-47C model rotor..

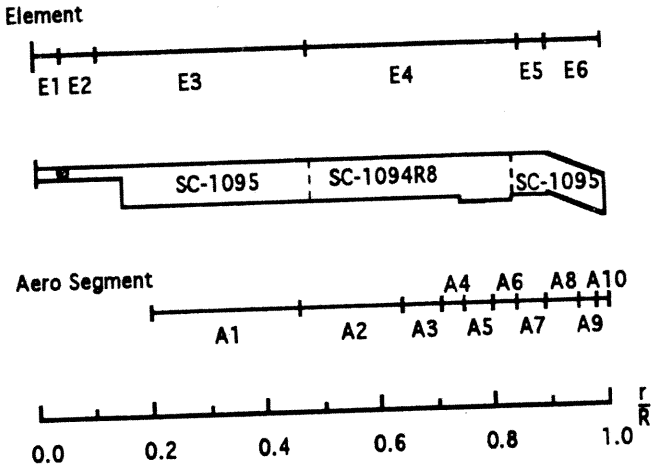

Fig. 11. UH-60A rotor blade geometry.

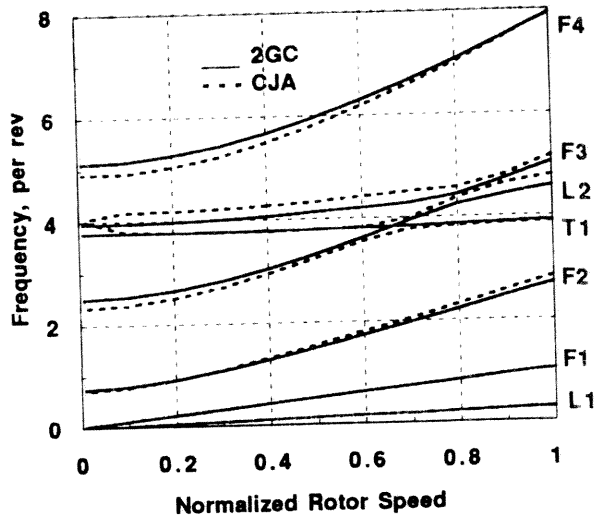

Fig. 12. UH-60A rotor blade frequencies, *in vacuo*.

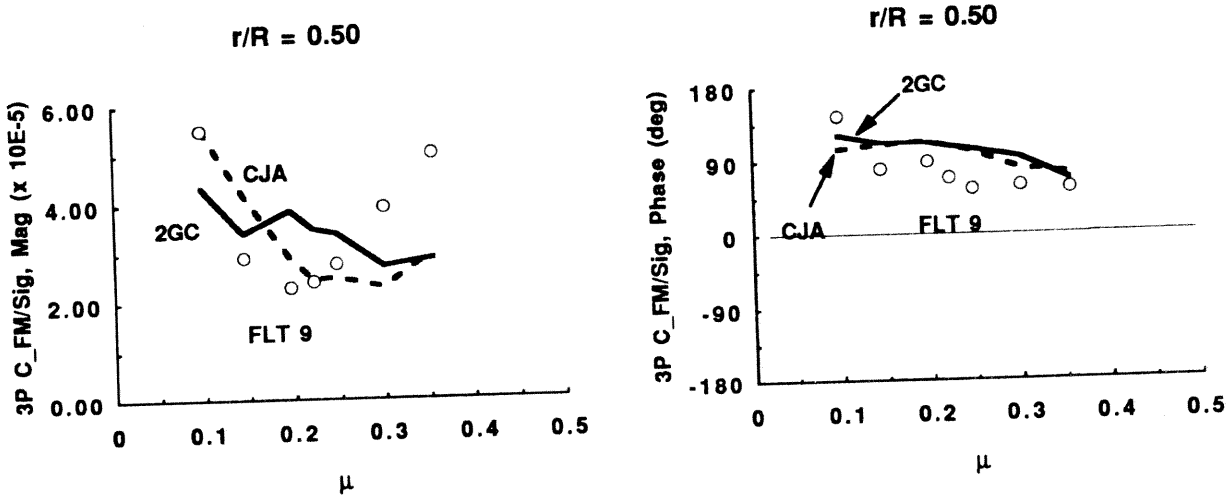

Fig. 13. UH-60A Black Hawk Phase 1, 3/rev blade loads

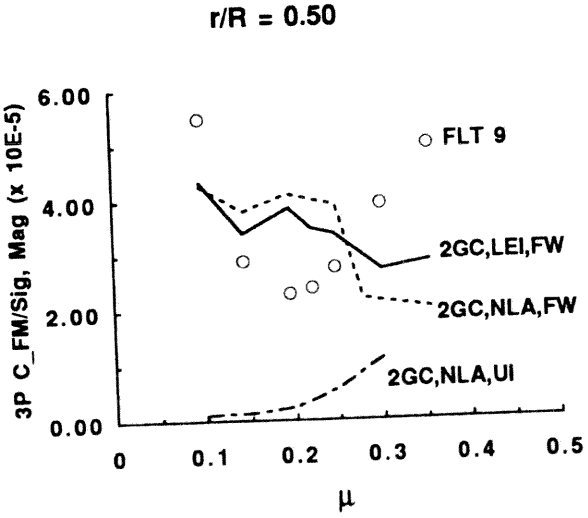

Fig. 14. Comparison of analytical variations in blade loads.

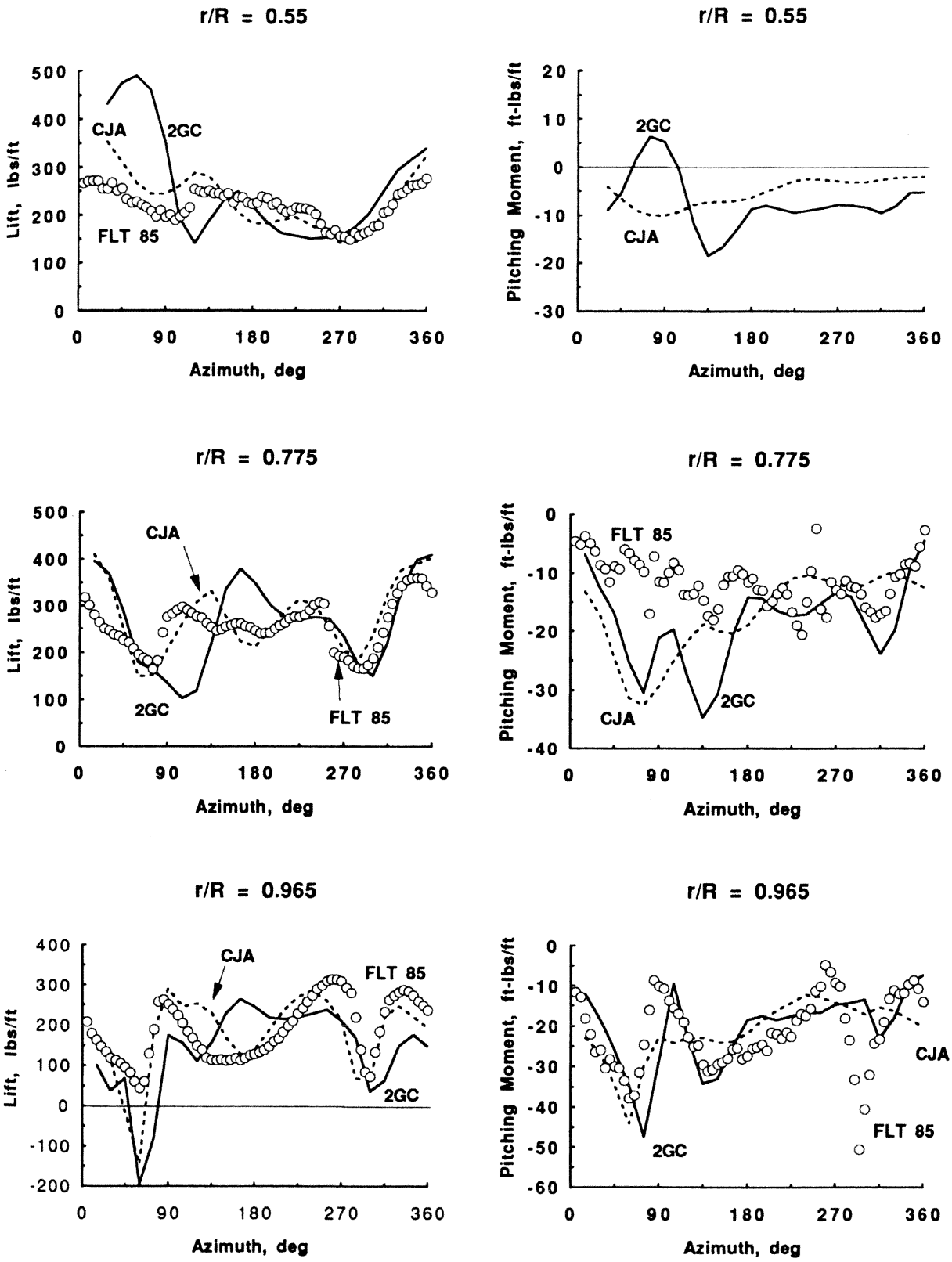

Fig. 15. UH-60A Black Hawk Phase 2 blade lift and moment airloads, advance ratio 0.105.

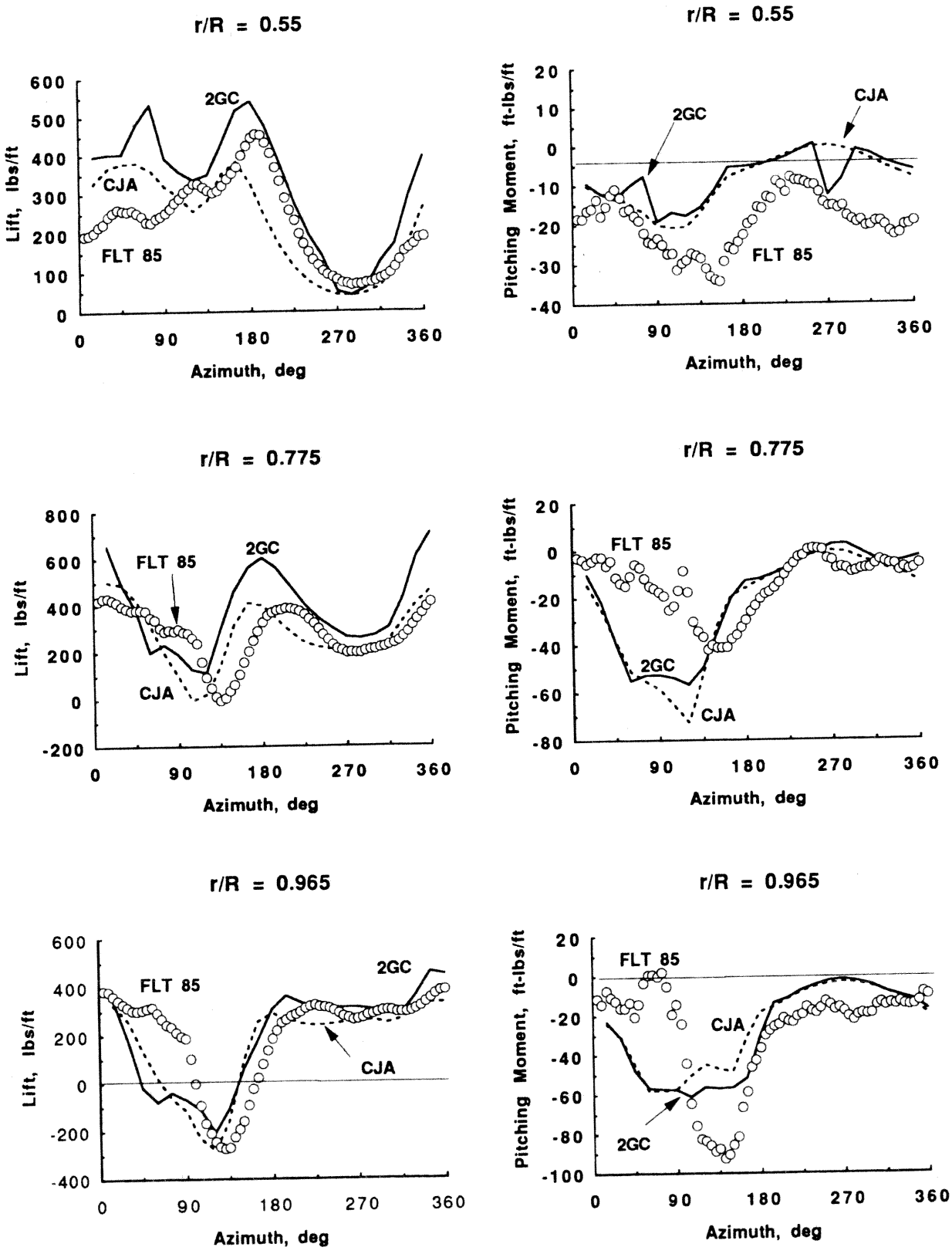

Fig. 16. UH-60A Black Hawk Phase 2 blade lift and moment airloads, advance ratio 0.368.

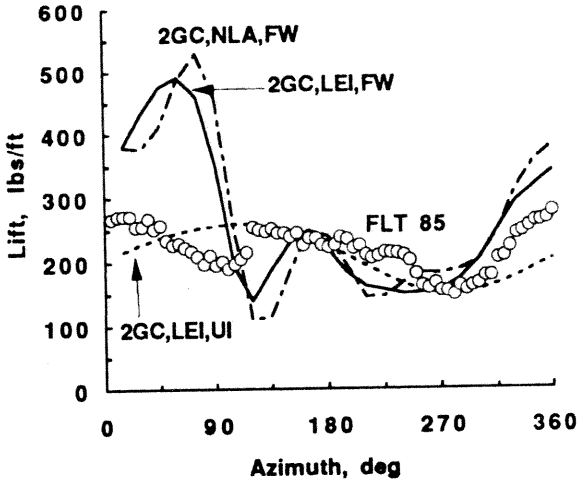

Fig. 17. Sensitivity of 2GCHAS blade lift airload predictions to aerodynamic modeling, 0.105 advance ratio, 55% span.

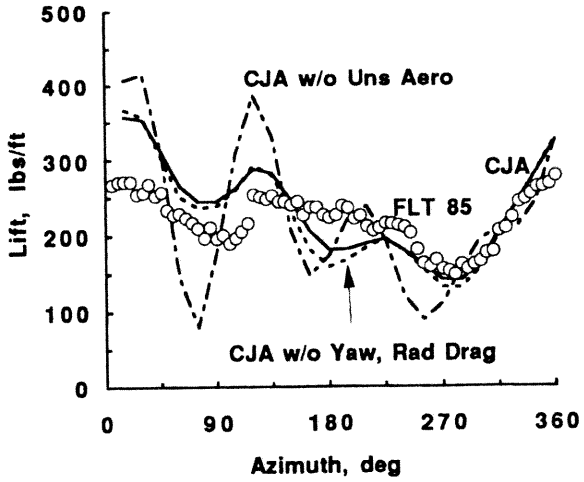

Fig. 18. Sensitivity of CAMRAD/JA blade lift airload prediction to aerodynamic modeling, 0.105 advance ratio, 55% span.

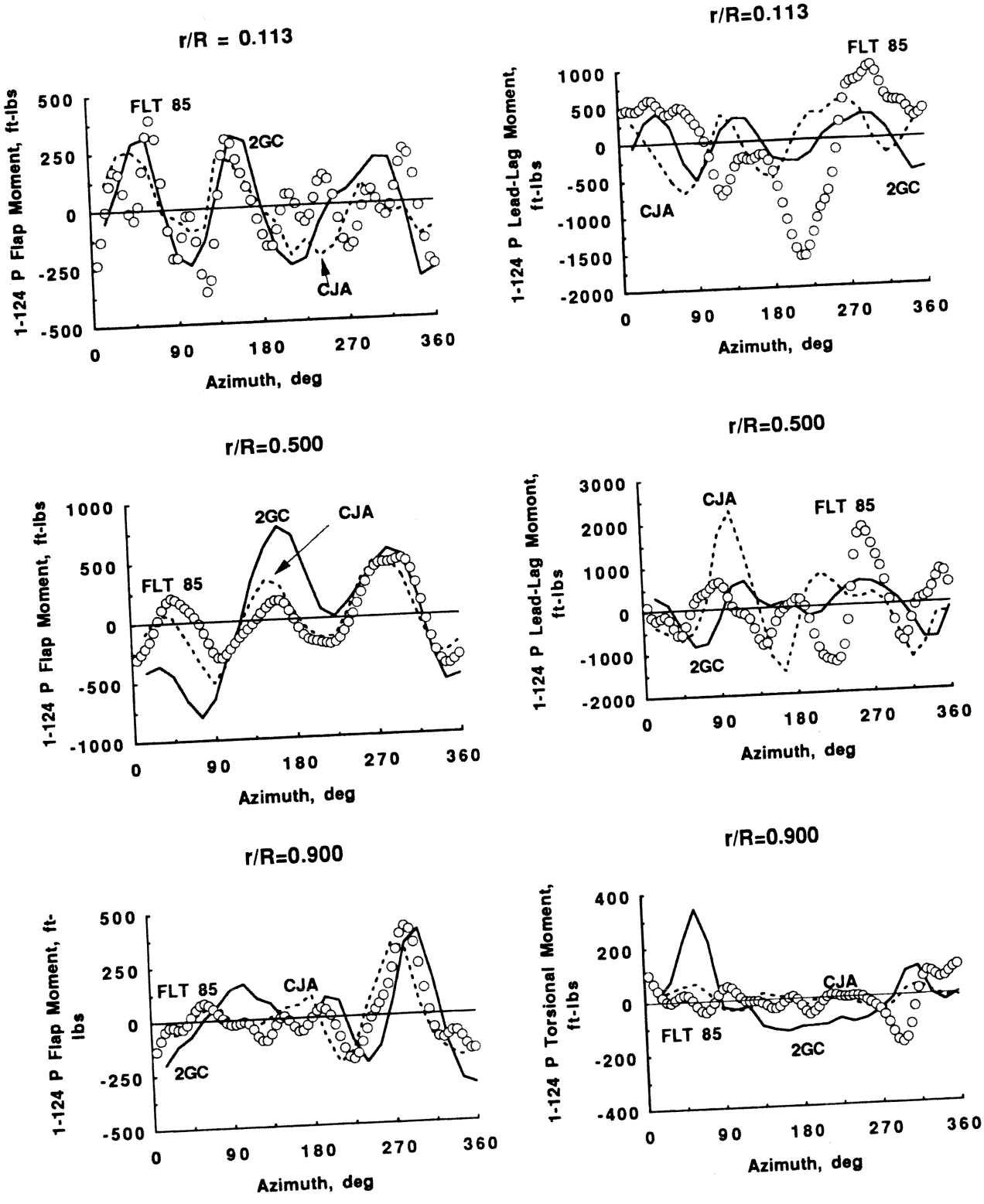

Fig. 19. UH-60A Black Hawk Phase 2 rotor blade bending and torsion moments at 0.105 advance ratio.

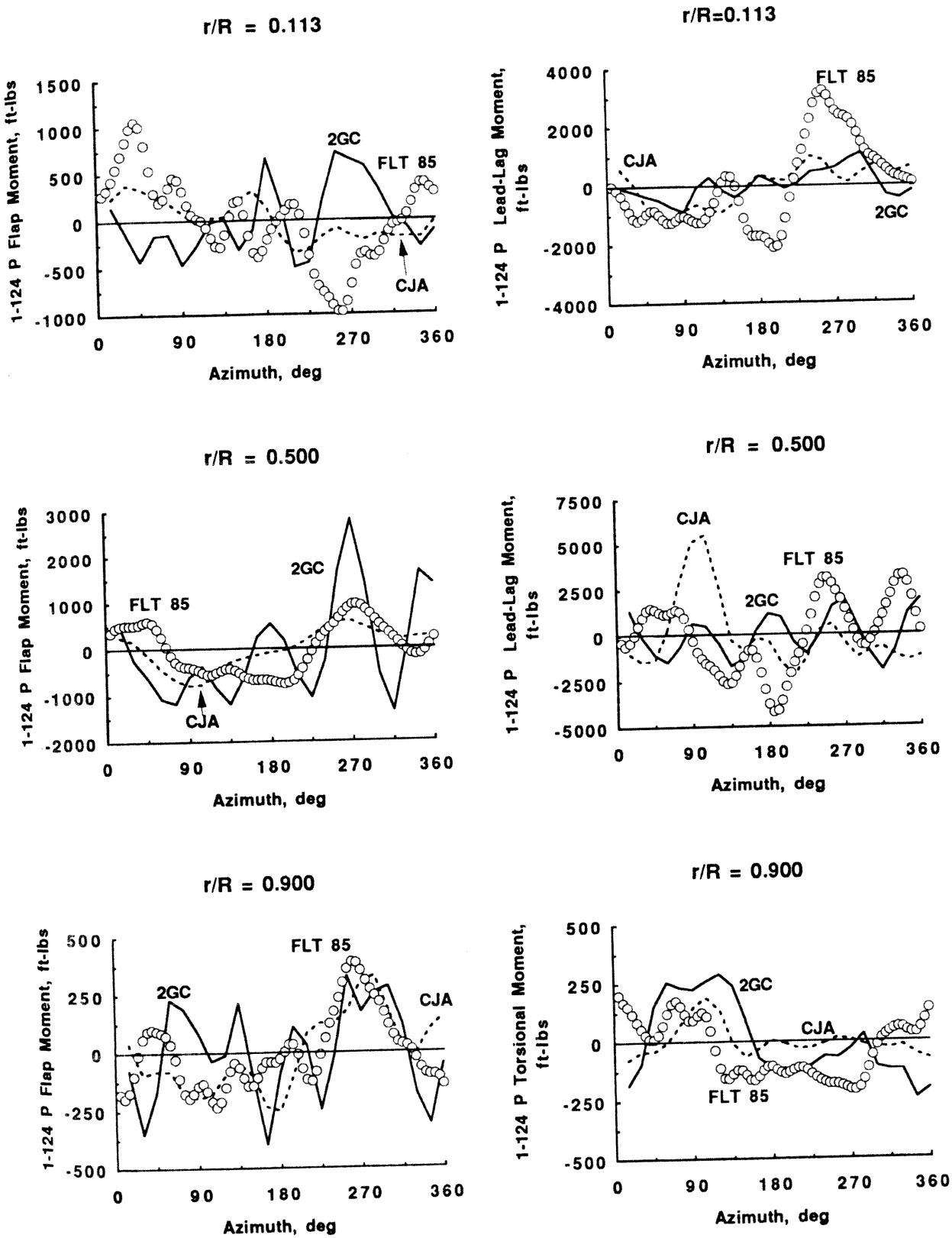

Fig. 20. UH-60 Black Hawk Phase 2 blade bending and torsion moments at 0.368 advance ratio.